Research Article | Vol. 25, No. 12 | 12 June 2017 | OPTICS EXPRESS 13252
Optics EXPRESS

Experimental parametric study of 128 Gb/s PAM-4 transmission system using a multi-electrode silicon photonic Mach Zehnder modulator

ALIREZA SAMANI,[1,2,3] DAVID PATEL,[1,2,4] MATHIEU CHAGNON,[1] ESLAM EL-FIKY,[1] RUI LI,[1] MAXIME JACQUES,[1] NICOLÁS ABADÍA,[1] VENKAT VEERASUBRAMANIAN,[1] AND DAVID V. PLANT[1]

[1]*Photonic Systems Group, Department of Electrical and Computer Engineering, McGill University, Montreal, Quebec, H3A 0E9, Canada*
[2]*Authors have equal contribution*
[3]*alireza.samani@mail.mcgill.ca*
[4]*david.patel@mail.mcgill.ca*

Abstract: We present an experimental study and analysis of a travelling wave series push-pull silicon photonic multi-electrode Mach-Zehnder modulator (ME-MZM) and compare its performance with a single-electrode travelling wave Mach-Zehnder modulator (TWMZM). Utilizing the functionality of the ME-MZM structure plus digital-signal-processing, we report: 1) the C-band transmission of 84 Gb/s OOK modulated data below the KP4 forward error correction threshold with 2 V_{pp} drive voltage over a distance of 2 km; 2) the transmission of a 128 Gb/s optical 4-level pulse amplitude modulated signal over 1 km of fiber; and 3) the generation of a 168 Gb/s PAM-4 signal using two electrical OOK signals. By comparing the transmission system performance measurements for the ME-MZM with measurements performed using a similar series push-pull TWMZM, we show that the ME-MZM provides a clear advantage in achieving higher baud PAM-4 generation and transmission compared to a TWMZM.

OCIS codes: (130.3120) Integrated optics devices; (230.2090) Electro-optical devices; (230.4110) Modulators; (200.4650) Optical interconnects.

References and links

1. D. Miller, "Device requirements for optical interconnects to silicon chips," Proc. IEEE **97**(7), 1166–1185 (2009).
2. IEEE P802.3bs 400 GbE Task Force, http://www.ieee802.org/3/bs/index.html
3. M. M. Fard, G. Cowan, and O. Liboiron-Ladouceur, "Responsivity optimization of a high-speed germanium-on-silicon photodetector," Opt. Express **24**(24), 27738–27752 (2016).
4. H. Chen, P. Verheyen, P. De Heyn, G. Lepage, J. De Coster, S. Balakrishnan, P. Absil, W. Yao, L. Shen, G. Roelkens, and J. Van Campenhout, "–1 V bias 67 GHz bandwidth Si-contacted germanium waveguide p-i-n photodetector for optical links at 56 Gbps and beyond," Opt. Express **24**(5), 4622 (2016).
5. P. Dong, L. Chen, and Y. K. Chen, "High-speed low-voltage single-drive push-pull silicon Mach-Zehnder modulators," Opt. Express **20**(6), 6163–6169 (2012).
6. R. Ding, Y. Liu, Y. Ma, Y. Yang, Q. Li, A. Lim, G. Lo, K. Bergman, T. Baehr-Jones, and M. Hochberg, "High-speed silicon modulator with slow-wave electrodes and fully independent differential drive," J. Lightwave Technol. **32**(12), 2240–2247 (2014).
7. D. Petousi, L. Zimmermann, A. Gajda, M. Kroh, K. Voigt, G. Winzer, B. Tillack, and K. Petermann, "Analysis of optical and electrical tradeoffs of traveling-wave depletion-type Si Mach–Zehnder modulators for high-speed operation," IEEE J. Sel. Top. Quantum Electron. **21**(4), 199–206 (2015).
8. M. Chagnon, M. Morsy-Osman, D. Patel, V. Veerasubramanian, A. Samani, and D. Plant, "Digital signal processing for dual-polarization intensity and interpolarization phase modulation formats using Stokes detection," J. Lightwave Technol. **34**(1), 188–195 (2016).
9. D. Patel, S. Ghosh, M. Chagnon, A. Samani, V. Veerasubramanian, M. Osman, and D. V. Plant, "Design, analysis, and transmission system performance of a 41 GHz silicon photonic modulator," Opt. Express **23**(11), 14263–14287 (2015).

#291039
Journal © 2017
https://doi.org/10.1364/OE.25.013252
Received 29 Mar 2017; revised 4 May 2017; accepted 4 May 2017; published 1 Jun 2017

Optics EXPRESS

10. A. Samani, M. Chagnon, D. Patel, V. Veerasubramanian, S. Ghosh, M. Osman, Q. Zhong, and D. Plant, "A low-voltage 35-GHz silicon photonic modulator-enabled 112-Gb/s transmission system," IEEE Photonics J. **7**(3), 1–13 (2015).
11. D. Patel, A. Samani, V. Veerasubramanian, S. Ghosh, and D. Plant, "Silicon photonic segmented modulator-based electro-optic DAC for 100 Gb/s PAM-4 generation," IEEE Photonics Technol. Lett. **27**(23), 2433–2436 (2015).
12. A. Shastri, C. Muzio, M. Webster, G. Jeans, P. Metz, S. Sunder, B. Chattin, B. Dama, and K. Shastri, "Ultra-low-power single-polarization QAM-16 generation without DAC using a CMOS photonics based segmented modulator," J. Lightwave Technol. **33**(6), 1255–1260 (2015).
13. A. Samani, V. Veerasubramanian, E. El-Fiky, D. Patel, and D. V. Plant, "A silicon photonic PAM-4 modulator based on dual-parallel Mach–Zehnder interferometers," IEEE Photonics J. **8**(1), 1–10 (2016).
14. R. Dubé-Demers, S. LaRochelle, and W. Shi, "Low-power DAC-less PAM-4 transmitter using a cascaded microring modulator," Opt. Lett. **41**(22), 5369–5372 (2016).
15. M. Hai, M. Fard, and O. Liboiron-Ladouceur, "A ring-based 25 Gb/s DAC-less PAM-4 modulator," IEEE J. Sel. Top. Quantum Electron. **22**(6), 123–130 (2016).
16. Y. Ehrlichman, O. Amrani, and S. Ruschin, "Improved digital-to-analog conversion using multi-electrode Mach–Zehnder interferometer," J. Lightwave Technol. **26**(21), 3567–3575 (2008).
17. M. Chagnon, M. Osman, M. Poulin, C. Latrasse, J. F. Gagné, Y. Painchaud, C. Paquet, S. Lessard, and D. Plant, "Experimental study of 112 Gb/s short reach transmission employing PAM formats and SiP intensity modulator at 1.3 μm," Opt. Express **22**(17), 21018–21036 (2014).
18. L. Chen, P. Dong, and Y.-K. Chen, "Chirp and dispersion tolerance of a single-drive push-pull silicon modulator at 28 Gb/s," IEEE Photonics Technol. Lett. **24**(11), 936–938 (2012).
19. M. Chagnon, S. Lessard, and D. Plant, "336 Gb/s in direct detection below KP4 FEC threshold for intra data center applications," IEEE Photonics Technol. Lett. **28**(20), 2233–2236 (2016).
20. E. El-Fiky, M. Chagnon, M. Sowailem, A. Samani, M. Morsy-Osman, and D. Plant, "168 Gb/s single carrier PAM4 transmission for intra data center optical interconnects," IEEE Photonics Technol. Lett. **29**(3), 314–317 (2017).

1. Introduction

Silicon photonics (SiP) has garnered immense interest as a suitable platform for the next generation of short reach optical interconnects. The low fabrication cost, high yield, small footprint, and complimentary metal-oxide semiconductor (CMOS) compatibility of the SiP platform makes it an attractive candidate for high-volume production of transmitter optical sub assembly (TOSA) and receiver optical sub-assemblies (ROSA) that would fit within the dimensions of a compact Quad Small Form-factor Pluggable (QSFP) module [1].

With the deployment of 100G and the development of 400G systems, there is a clear need for high bandwidth and power efficient modulators and photodetectors. As per recent IEEE taskforce discussions, 400 Gb/s PSM-4 systems will be realized using 1λ × 4 fibers × 50 Gbaud PAM-4 configurations [2], where the increased spectral efficiency of PAM-4 compared to OOK enables 100 Gb/s transmission per fiber. Recently, high bandwidth and high responsivity silicon germanium (SiGe) photodetectors that can meet the required specifications for 100 Gb/s ROSAs have been demonstrated [3,4], and considerable work has also been done on SiP modulators [5–7].

To realize 400G systems several recent studies have demonstrated that high bandwidth (BW) SiP modulators can be utilized to achieve single channel 100 Gb/s transmission [8–10]. However, the presented SiP modulators were designed with the OOK modulation format as their target application and relied on electronics for the generation of 4-level intensity modulated signals. Recent studies have shown that PAM-4 transmission can be achieved using OOK signals with different modulator architectures such as multi-electrode Mach-Zehnder modulators (ME-MZM) [11,12], and dual-parallel Mach-Zehnder modulators (DP-MZM) [13]. We experimentally showed that these modulators can be driven using conventional pulse pattern generators and an electrical OOK format to generate PAM-4 signals. Recent studies have also shown that resonant devices including cascaded ring resonators and ring-assisted MZI modulators are capable of optical PAM-4 generation [14,15].

In this paper, we present a series push-pull (SPP) silicon photonic Multi-Electrode Mach-Zehnder modulator (ME-MZM) with a 3-dB EO bandwidth greater than 45 GHz. We present

Optics EXPRESS

the analytical study of the modulator, and its small and large signal characterization. The linearity of the transfer function of the ME-MZM along with the PN junction phase shifters are investigated. We next experimentally demonstrate the generation of 168 Gb/s PAM-4 signals using the ME-MZM driven by two OOK electrical signals which are conditioned using minimal digital signal processing (DSP) which includes pulse shaping at symbol rates up to 84 Gbaud, RF spectral pre-compensation filter, clipping, and quantization. Furthermore, we investigate the transmission performance of the ME-MZM compared to a conventional SiP SPP travelling wave Mach-Zehnder modulator (TWMZM) over various lengths of fiber. This allows us to quantitatively compare the PAM-4 signal generation in optical domain achieved by utilizing the ME-MZM, versus TWMZM which requires the PAM-4 signal to be generated in electrical domain. In addition we study the transmission performance improvements achieved by using DSP. We report successful transmission of 128 Gb/s PAM-4 over 2 km of fiber below the KP4 forward Error correction (FEC) threshold of 2.0×10^{-4} in C-band. We show that ME-MZM can achieve higher bit rate transmission due to the higher bandwidth of each segment compared to a similar TWMZM. Additionally we experimentally demonstrate that by utilizing ME-MZM functionality which requires only OOK drive signals, higher baud PAM-4 generation can be achieved. We further present the power consumption per bit of each modulator for various bitrates and modulation formats. The result of this analysis shows that ME-MZM offers a more efficient solution for higher baud PAM-4 compared to TWMZM.

2. Device design and characterization

In this section, we present the device design, DC, and small signal characterization of the ME-MZM. Furthermore, we compare the performance of the device with a SPP TWMZM. The schematic of the structure and the analytical model of a loss less ME-MZM are presented in Fig. 1.

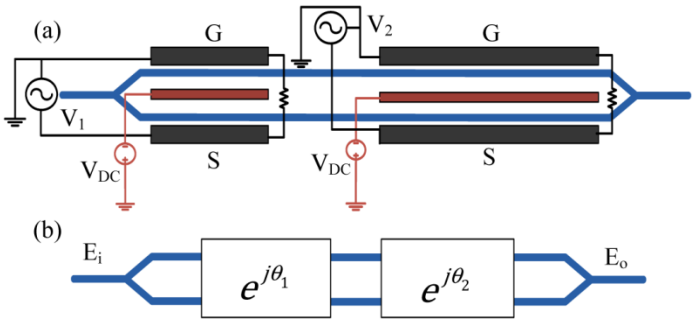

Fig. 1. (a) The schematic of the structure and (b) analytical model of a SPP ME-MZM.

Since the two segments of the ME-MZM can be driven independently, the output electric field of ME-MZM can be written as:

$$E_o = \frac{E_i}{2} e^{j(\theta_1+\theta_2)} \tag{1}$$

Where, E_i is the input electric field, θ_1 and θ_2 are the phase changes from modulating each segment. From (1), the output light intensity of the ME-MZM, ignoring loss, is:

$$I_o = \frac{|E_i|^2}{2}(1+\cos(\theta_1+\theta_2)) \tag{2}$$

Figure 2 illustrates the micrograph of the ME-MZM and TWMZM. The electrode design and the PN junction of the modulators are identical to each other and are presented in detail in

Optics EXPRESS

[10]. Both devices were fabricated on a silicon on insulator (SOI) wafer, with a 220 nm silicon layer thickness and a 2 μm thick buried oxide layer in the same fabrication run at IME A*STAR. The ME-MZM is designed such that equally spaced PAM-4 amplitude levels are achieved using two binary electrical driving signals with the same peak to peak amplitude. To implement this, the longer segment of the ME-MZM is twice the length of the shorter segment. This will result in the longer segment having a V_π value that is one half of the shorter segment's V_π .

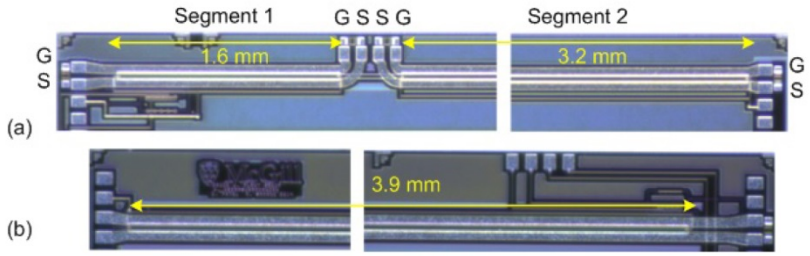

Fig. 2. Micrograph of (a) the ME-MZM and (b) the TWMZM.

Since each individual segment of the ME-MZM can be driven independently, the device can operate as a 2 bit optical digital to analog convertor (DAC) to generate PAM-4 signals while driven by two OOK electrical signals. Ideally, when both segments of the ME-MZM are driven by the signals with the same peak to peak amplitude, the phase shift value of the longer segment would be double that of the shorter segment. Figure 3(a) illustrates the measured phase shift for each segment of the ME-MZM and the TWMZM. The optical power transmission of the ME-MZM as a function of the phase shift of each segment and the transfer function of the ME-MZM is shown in Figs. 3(b) and 3(c) respectively. As shown in Figs. 3(a)-3(c) the SiP ME-MZM suffers from a higher non-linearity than an ideal case. To improve the linearity of the modulator and to realize equally spaced PAM-4 amplitude levels, the drive voltage dynamic range (DR) should be adjusted to the linear region of the transfer function [16]. This is achieved by properly biasing the segments of the ME-MZM to the midpoint of the transfer function as well as reducing the drive voltages of each segment. By limiting the DR of the modulator to 0.6π as shown in Fig. 3(c) using the red dashed line; the measured integral and differential non-linearity of the ME-MZM as a 2 bit DAC are 0.315 and 0.35 for full DR and 0.15 and 0.075 for the operating DR presented in Fig. 3(c) respectively.

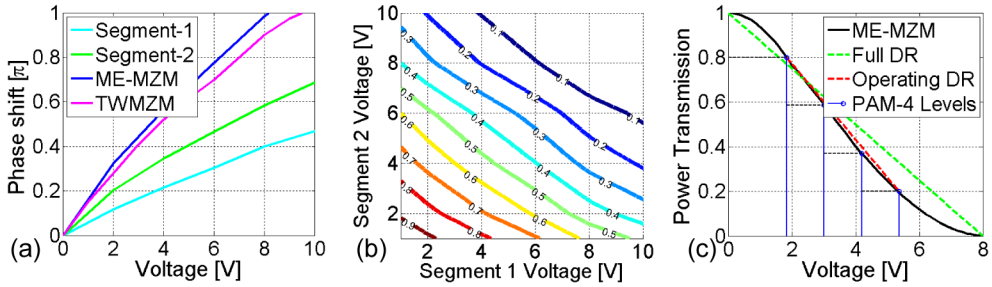

Fig. 3. Measured values of the: (a) Phase shift vs. voltage of ME-MZM and TWMZM, (b) the optical power transmission of the presented ME-MZM as a function of the voltage applied to each segment and (c) transfer function of the SiP ME-MZM (ignoring losses).

The insertion loss of the ME-MZM and TWMZM are measured to be 4.3 and 3.3 dB, respectively. Vertical shallow etched grating couplers are used to couple light in and out of the SiP chip. A 14 dBm tunable laser is used as an input for the modulators. All travelling wave electrodes of both modulators are terminated using external 50 GHz, 50 Ω termination

Optics EXPRESS

through the RF probes. A 200 μm intrinsic section is placed between the two phase shifter segments of the ME-MZM, to isolate the two segments and accommodate the input and termination of each electrode. The electro-optic (EO) response of each segment of the ME-MZM are measured using a Lightwave Component Analyzer (LCA) and are shown in Fig. 4(a). Similarly the EO S21 response of the TWMZM is shown in Fig. 4(b). The electrical input of the modulator is connected to the RF port 1 of the LCA, and the modulated output optical signal is connected to the optical receiver port of the LCA. The noise floor of the LCA's measurements is reported to be < - 59 dB (W/A) at 50 GHz for EO measurements. The travelling wave electrodes of both modulator were terminated using an external 50 ohm termination through the RF probes. Due to the shorter length of the ME-MZM electrodes, lower microwave attenuation and lower velocity mismatch, the EO 3-dB bandwidth of the ME-MZM segments are significantly higher than the TWMZM. In addition due the extra electrode routing the total electrode length of the TWMZM is 4.5 mm which results in higher loss. Consequently the higher achievable bandwidth of the ME-MZM will allow the modulator to achieve higher modulation rates. It should be noted that by decreasing the length of the TWMZM the bandwidth of the device can be improved however this will result in higher V_π. The electrical S11 of the ME-MZM segments and the TWMZM are shown in Figs. 4(c) and 4(d) respectively.

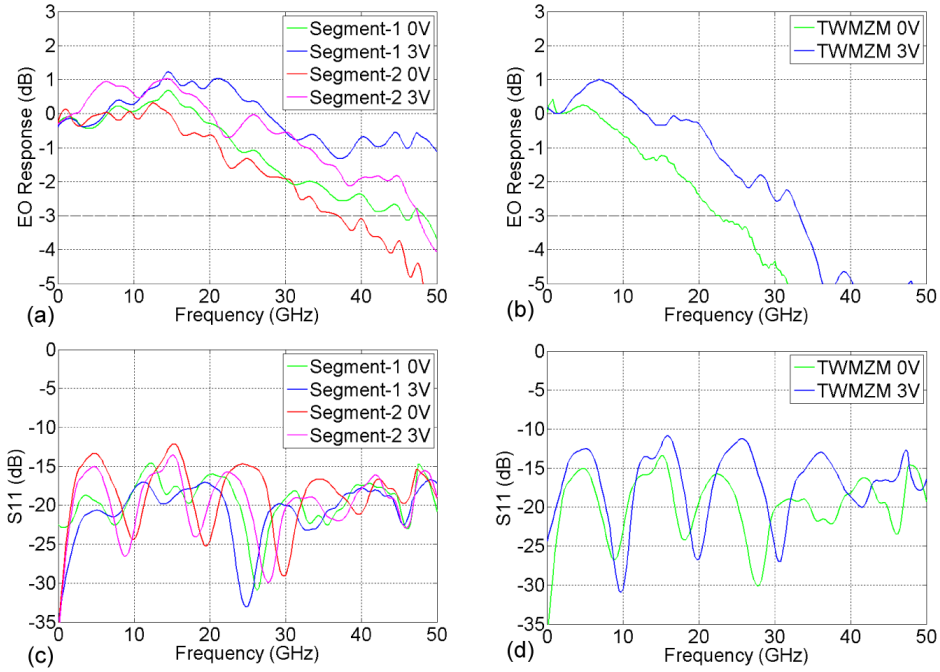

Fig. 4. Electro-optic response of the (a) ME-MZM and (b) TWMZM, and the electrical S11 response of the (c) ME-MZM and (d) TWMZM.

3. Large signal and transmission experiment

As recent studies have shown, using DSP is a possible and in some cases necessary solution to achieve 50 Gbaud PAM-4 transmission [8–10]. In this section we compare the performance of both modulators and particularly focus on the transmission improvement achieved using DSP on the transmitted and received signal. We parametrically investigate the large signal transmission performance of the TWMZM and ME-MZM under two conditions. First in *condition 1*, the large signal performance of the devices without any DSP is presented, using a pulse pattern generator (PPG) to operate the modulators. In this setup, we use the optical

Optics EXPRESS

sampling head of the digital communication analyzer (DCA) as the receiver as shown in Figs. 5(a)-5(c). Next in *condition 2*, we present the large signal performance with offline DSP using an electrical digital-to-analog convertor (DAC) and an analog-to-digital convertor (ADC). The transmission performance of the devices is investigated by applying DSP on both the transmitted signal and the received signal. To perform error counting and apply DSP on the received signal in *condition* 2, instead of the DCA, a 50 GHz, 0.65 A/W photodetector is used for the optical to electrical conversion, and a real-time oscilloscope is used to capture the transmitted data and perform error counting. In *condition* 1, we use binary electrical signals to drive the modulator, hence in the case of the TWMZM, PAM-4 operation could not be achieved. In the second *condition*, we investigate the PAM-4 performance of each device. Specifically, we investigate the quality of the signals when the PAM-4 levels are generated in the electrical domain using the electrical DAC and they are applied to the TWMZM versus when the PAM-4 levels are generated in the optical domain using the ME-MZM structure.

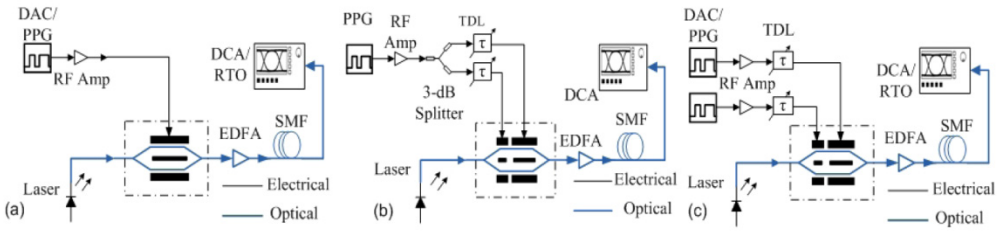

Fig. 5. Schematic of the experimental setup for (a) OOK and PAM-4 modulation using TWMZM (b) OOK modulation using ME-MZM and (c) PAM-4 modulation using ME-MZM.

3.1 Condition 1: Transmission without DSP

For OOK transmission in condition 1, a pseudo random bit sequence (PRBS)-31 signal from the PPG is amplified using a 40 GHz RF amplifier. In the case of the TWMZM, the driving signal is applied directly to the modulator after amplification. Figure 5(a) illustrates the experimental setup schematic for OOK modulation using the TWMZM. When driving the ME-MZM as shown in Fig. 5(b), a single OOK signal is divided into two branches using a 50 GHz 3-dB splitter. Matched RF cables and RF amplifiers are used to ensure that both signals have the same RF path length and tunable delay lines are used to time align the two signals such that the signal driving the second segment has a delay equal to the length of the first segment plus the intrinsic section separating the two segments. This delay can be calculated by dividing the first segment length (1.6 mm) plus the intrinsic section (0.2 mm) by group velocity of the optical mode. In this configuration, both segments are operated using the same driving voltage. Figure 5(c) describes the configuration used to generate PAM-4 signals using the ME-MZM. In this scenario, two independent OOK PRBS signals are generated using the PPG and applied to each segment of the ME-MZM. To compensate for the nonlinearity of the phase shifters shown in Fig. 2(a) and to obtain equally spaced PAM-4 levels, the drive signal for the longer segment is amplified to 5 V_{pp} and the signal driving the shorter segment is amplified to 3.8 $V_{pp.}$ Both segments of the modulator are biased at 3.5 V. The RF tunable delay lines are used to time align each signal visually using the DCA such that the bit transition of each signal overlaps. In all three configurations the modulated optical signal was then amplified using an EDFA, and propagated through various lengths of fiber. The 80 GHz optical sampling head of the DCA is used as the receiver. The received optical power is kept constant at 5 dBm. Figure 6 demonstrates the OOK eye diagrams of both the ME-MZM and TWMZM and the PAM4 eye diagram of ME-MZM at 40 Gbaud with their corresponding measured Q-factor and vertical eye closure penalty (VECP) values.

Optics EXPRESS

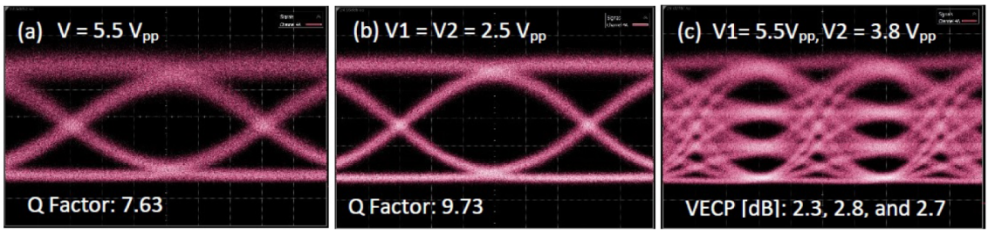

Fig. 6. 40 Gbaud OOK eye diagram of (a) TWMMZM (b) ME-MZM and (c) PAM-4 eye diagram of ME-MZM.

As shown in section 2 the higher bandwidth of the ME-MZM and longer effective phase shifter length should allow it to reach higher baud rates compared to the TWMZM, however to properly compare the two modulators we need to consider the operating conditions and the drive voltages applied to each modulator. To quantify the performance of each modulator under various drive voltages and symbol rates, we measure the Q-factor of the OOK eye diagram using the DCA. Additionally, for the PAM-4 modulation using ME-MZM, we estimate the BER performance at various symbol rates and transmission distances using the method presented in [17]. Figures 7(a) and 7(b) present the back to back OOK Q-factor of each modulator and Fig. 7(c) shows the PAM-4 BER of the ME-MZM over various fiber lengths. The dashed horizontal black lines in Figs. 7(b) and 7(c) represent the KP4 hard decision FEC threshold at 2.0×10^{-4}. When using OOK modulation, the bias voltage applied to both modulators is adjusted to $V_{pp}/2 + 0.5$ V to ensure that PN junctions are always in reverse bias. Referring to Fig. 7(a) it can be seen that the ME-MZM achieves a significantly higher Q factor than the TWMZM at the same drive voltages, however it should be noted that the ME-MZM is operated using 2 drive signals. The better performance of the ME-MZM can be attributed to its longer overall phase shifter length (approximately 1 mm longer) and the lower microwave loss of each segment compared to the TWMZM. In Fig. 7(c) the drive voltages for the short and long segments of the ME-MZM are 3.8 and 5 $V_{pp,}$ and we achieve a 50 Gbaud below FEC, PAM-4 transmission over 1 km of fiber without any DSP. We attribute the better performance of the modulator through 500 m of fiber compared to back to back transmission to the small negative chirp of the SPP modulators which results in compensating the fiber chromatic dispersion in fiber [13, 18]. These measurement results will be compared to the *condition* 2 results in the next section to quantify the improvement achieve using DSP.

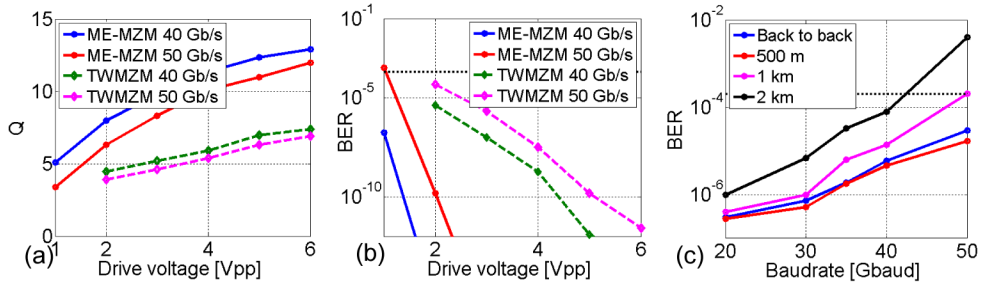

Fig. 7. Back to Back OOK Q-factor of (a) ME-MZM and TWMZM, (b) OOK BER of ME-MZM and TWMZM and (c) the PAM-4 BER of ME-MZM over various length of SMF.

3.2 Condition 2: Transmission with DSP

In condition 2, the PPG is replaced by the DAC as shown in Figs. 5(a) and 5(c). This study will allow us to quantify the improvements achieved by using DSP on transmission performance of each modulator. For OOK modulation, two identical PRBS signals are generated using two DAC channels. Matched RF cables along with TDLs are used to ensure

Optics EXPRESS

that the signals are time aligned. In this scheme, the RF 3-dB splitter is not required as the DAC can generate identical PRBS signals on different channels. The DAC operates at 1 sample per symbol at 84 GSamples/s. The transmitter DSP includes, symbol generation, pulse shaping at symbol rates up to 84 Gbaud, RF spectral pre-compensation filter up to the RF amplifier outputs, clipping, and quantization [19,20]. It is to be noted that pulse-shaping at 84 Gbaud is performed by the DAC with an appropriately chosen equalizer and without intentional pulse shaping in the digital domain. For PAM-4 transmission using TWMZM, the signal amplitude levels are adjusted using the DAC to compensate for the MZM transfer function and the RF amplifier's gain non-linearity. The generated signal is amplified to 5.5 V_{pp} and applied to the modulator. On the receiver side, we replace the DCA with a 50 GHz, 0.65 A/W photodetector for optical to electrical conversion and a 63 GHz real time oscilloscope (RTO) to capture the modulated signals and store it for the offline receiver DSP and error counting. The receiver DSP consists of: sampling the signal at 160 GSa/s, matched filtering at 2 × baud rate, clock recovery, followed by receiver equalizer and symbol decision. The received eye diagrams are generated offline using MATLAB. The driving signal amplitudes for 56 Gbaud are the same as the *condition* 1; however due to stronger equalization at 84 Gbaud, the maximum achievable peak-to-peak voltage after the RF amplifiers is 4 V_{pp} and as a result for PAM-4, the binary electrical signals applied to the shorter and longer segments are 3 and 4 V_{pp}, respectively. For OOK generation, the two signals driving each segment have the same amplitude. Figure 8 shows OOK and PAM-4 eye diagram of the ME-MZM at 56, and 84 Gbaud.

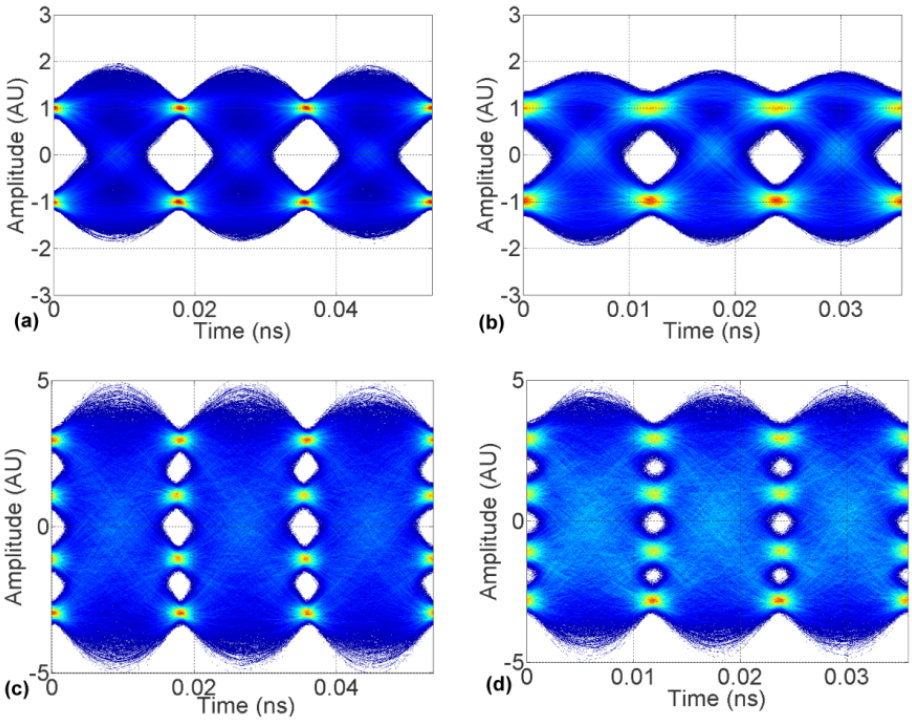

Fig. 8. (a) 56 Gbaud OOK, (b) 84 Gbaud OOK, (c) 56 Gbaud PAM-4 and (d) 84 Gbaud PAM-4 eye diagram of the ME-MZM.

Using the receiver DSP, we can further optimize the vertical decision making threshold for each PAM-4 level hence improving the performance of each device. We experimentally study three main parameters of the transmission system: 1) the modulator driving voltage, 2) the modulation baud rate and 3) the transmission distance for PAM-4. As shown in Fig. 9,

Optics EXPRESS

both modulators are capable of 84 Gbaud OOK transmission with Q factors that correspond to a BER below the FEC threshold. Figure 9(a) shows the 84 Gbaud OOK BER performance of each device for various transmission lengths and drive voltages. As demonstrated, ME-MZM performs noticeably better than the TWMZM. Similarly, we investigate the PAM-4 transmission performance of both devices for various baud rates and drive voltages in Figs. 9(b) and 9(c). It can be seen from Figs. 7 and 9, that using DSP, both modulators can be operated using lower drive voltages yet maintain the same BER performance.

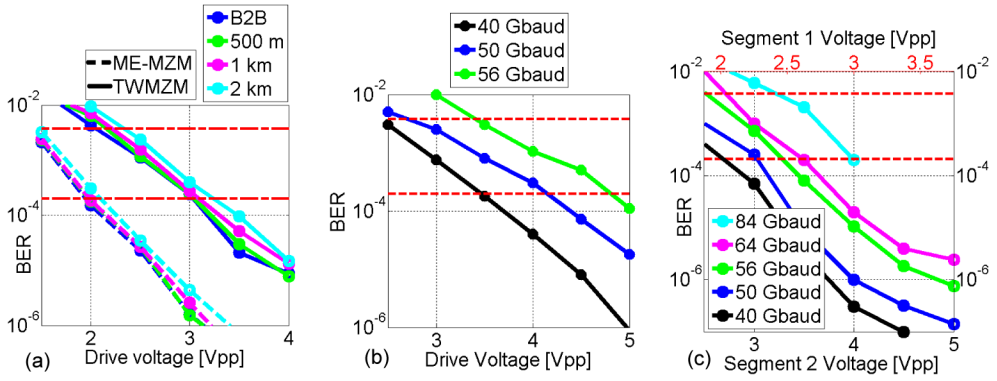

Fig. 9. OOK BER of (a) ME-MZM and TWMZM over various length of SMF, (b) PAM-4 BER of TWMZM, and (c) the PAM-4 BER of ME-MZM versus drive voltage. Dashed lines indicate the HD-FEC threshold of 3.8×10^{-3} and the KP-4 FEC threshold of 2.0×10^{-4}.

Several factors contribute to superior performance of the ME-MZM compared to TWMZM. First, the lower microwave loss of ME-MZM electrodes enable higher symbol rate operation compared to TWMZM. Additionally, the smaller length of the electrodes results in a lower velocity mismatch between the optical and microwave signals resulting in higher E-O bandwidth. We also note that the overall total phase shifter length of the ME-MZM is longer than the TWMZM, which results in a lower V_π for the device. However, this increase in length results in higher insertion loss compared to TWMZM.

As shown in section 2, ME-MZM generates PAM-4 signals by combining two OOK electrical driving signals in the optical domain. It should be noted that, in the electrical domain, the PAM-4 drive signals that the DAC generates have lower Q-factor than the OOK drive signals; as a result, the ME-MZM performs better since its structure enables it to be driven by better quality drive signal. With the ME-MZM, we achieve an 84 Gbaud PAM-4 generation below the KP-4 FEC threshold of 2.0×10^{-4}, which to the best of our knowledge, is the highest baud rate ever reported using a silicon photonic modulator. We further examine the transmission performance of the two devices over various lengths of single mode fiber. Figure 10 presents the BER performance of the system for various bauds and transmission distances. Two OOK signals of 4 V_{pp} and 3 $V_{pp,}$ amplitude are applied to the longer and shorter segment of the ME-MZM respectively, and the TWMZM is driven by a 5 V_{pp} PAM-4 signal.

Optics EXPRESS

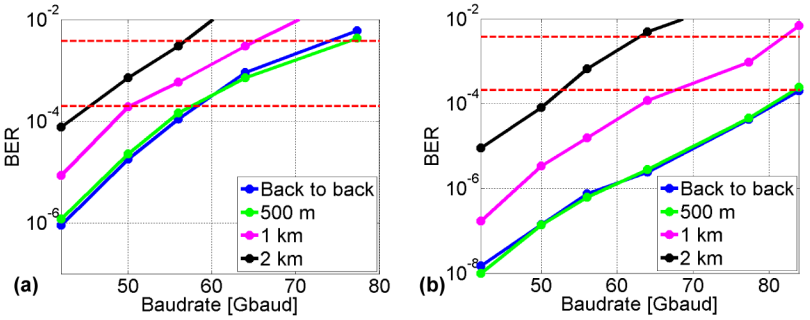

Fig. 10. BER performance of the (a) TWMZM and (b) ME-MZM for various bauds and transmission distances. Dashed lines indicate the HD-FEC threshold of 3.8×10^{-3} and the KP-4 FEC threshold of 2.0×10^{-4}.

Using the ME-MZM, we report a successful transmission of 56 Gbaud PAM-4 signal over 1 km of SMF below KP4 FEC threshold. As both devices are designed for C-band operation, at higher distances, the BER is significantly affected by the fiber chromatic dispersion. We expect an O-band device to perform considerably better at higher distances.

Assuming the power consumption is dominated by the resistive loss, we estimate the energy per bit consumption of both modulators using the method shown in [9]. The power consumed by each electrode can be estimated by $P = \sum_{i=1}^{N} \frac{V_{i,RMS}^2}{R}$, where, N is the number of segments or electrodes and V_{rms} is the root-mean-square of the voltage driving the i^{th} segment. Table 1 presents the lowest power consumption per bit (pj/bit) of each modulator at different bauds achieving a BER below the KP4 FEC threshold. It is to be noted that the power consumption reported is only for the modulator itself.

It can be seen that at lower bauds, and OOK format, TWMZM provides a more efficient option compared to ME-MZM. This is due to that fact that ME-MZM requires 2 driving signals. However, using PAM-4 modulation and higher bauds, ME-MZM provides an advantage over TWMZM. At 56 Gbaud PAM-4 the ME-MZM energy consumption per bit is estimated to be 0.41 pj/bit while TWMZM's power consumption is 0.56 pj/bit. To achieve a higher PAM-4 baud using a TWMZM, a significantly higher drive voltage is required to compensate for the lower bandwidth of the device. However ME-MZM can be driven by considerably lower drive voltages. Furthermore, the length of the ME-MZM segments can be optimized for a certain baud to allow for the most efficient power consumption.

Table 1. Power consumption per bit (pj/bit) of each modulator.

Baud [Gbaud]	ME-MZM				TWMZM			
	OOK, V_{rms1}, V_{rms2} [V]	OOK (pj/bit)	PAM-4, V_{rms1}, V_{rms2} [V]	PAM-4 (pj/bit)	OOK, V_{rms} [V]	OOK (pj/bit)	PAM-4, V_{rms} [V]	PAM-4 (pj/bit)
40	0.53, 0.53	0.28	1.06, 0.80	0.44	0.70	0.25	1.24	0.38
50	0.53, 0.53	0.22	1.23, 0.88	0.46	0.70	0.2	1.59	0.51
56	0.53, 0.53	0.20	1.23, 0.88	0.41	0.70	0.18	1.767	0.56

4. Conclusion

We present the design, analysis and transmission performance of a multi electrode Mach Zenhnder modulator for multi amplitude optical signal generation. We achieve the highest reported PAM-4 signal generation of 168 Gb/s using 2 OOK electrical drive signals using

Optics EXPRESS

DSP. We further investigate the transmission properties of the device under various driving conditions and compare the performance of the device with a similar TWMZM. We experimentally show that ME-MZM structure enables higher baudrate transmission due to its higher electro-optic bandwidth compared to a similar single electrode TWMZM. Without any digital signal processing and using a conventional PPG, the ME-MZM is capable of generating 100 Gb/s PAM-4 signal. A 128 Gb/s PAM-4 transmission over 1 km of SMF is also presented which to best of our knowledge is the higher reported PAM-4 baud transmission using a SiP modulator.

5. Acknowledgements

This work was supported in part by the Natural Sciences and Engineering Research Council of Canada (NSERC).